Polarizability of Kr^{6+} from high-L Kr^{5+} fine-structure measurements

S. R. Lundeen
Department of Physics, Colorado State University, Ft. Collins, Colorado 80523, USA

C. W. Fehrenbach
J.R. Macdonald Laboratory, Kansas State University, Manhattan, Kansas 66506, USA

(Received 21 February 2007; published 30 March 2007)

The transition between $n=55$ and $n=109$ Rydberg levels of Kr^{5+} has been studied at high resolution using the resonant excitation stark ionization spectroscopy method. Resolved excitation of $L=6$, 7, 8, and 9 levels in $n=55$ lead to a determination of the fine-structure energies of these levels. Interpreted with the long-range polarization model, this leads to a measurement of the dipole polarizabilities of Zn-like Kr^{6+}, $\alpha_d=2.69(4)a_0^3$. Obtaining a value of the quadrupole polarizability from the data will require additional theoretical input. Factors contributing to the signal and noise levels in measurements of this type are discussed.

DOI: 10.1103/PhysRevA.75.032523 PACS number(s): 32.10.Dk, 32.10.Fn, 32.30.Bv

I. INTRODUCTION

Fine structure patterns in nonpenetrating high-L Rydberg states of atoms and ions reflect the long-range interactions between the Rydberg electron and the ion core that break the L-degeneracy characteristic of pure Coulomb attraction. In the case of S-state ion cores, the pattern is largely due to the dipole polarizability of the ion core, with smaller contributions from higher order multipole polarizabilities and nonadiabatic corrections. In the more general case when the core ion has nonzero angular momentum, more complex fine-structure patterns occur that contain contributions from the permanent electric moments of the core ion. When these patterns can be measured in states of sufficiently high L, they provide a way to determine numerous properties of the core ion. These measurements can check *a priori* calculations and may also be useful in empirical descriptions of the long-range interactions of the core ion in other applications [1]. In order to extract these core properties with confidence, it is necessary to have measurements of fine-structure energies across a wide range of Rydberg angular momentum L so as to unambiguously separate the contributions to the fine structure from the various contributing effects, which generally have different dependences on L.

One experimental technique that is particularly suited in this regard is the resonant excitation stark ionization spectroscopy (RESIS) method, in which the Rydberg levels are formed by charge capture in a wide range of L levels and detected by upwards excitation with a Doppler-tuned CO_2 laser followed by Stark ionization. With this method, no selection rules limit the range of L levels that can be detected. In practice, since the fine-structure energies decrease rapidly with L, the frequency resolution of the laser excitation sets an upper limit to the range of L's that can be distinguished. Two recent examples of the use of this method to measure high-L fine-structure patterns and extract core ion properties are the study of $n=29$, $8\leqslant L\leqslant 8$ fine-structure energies in Si^{2+} [2] and the study of $n=10$, $5\leqslant L\leqslant 8$ fine-structure energies in Ne [3].

The use of the RESIS method to study fine structure in Rydberg ions has been reported previously in only two cases [2,4]. It depends critically on the physics of resonant charge capture, which allows the selective population of highly excited Rydberg ions bound by approximately one CO_2 photon, or about 0.10 eV, regardless of the charge of the ion. In the work reported here, highly excited states of Kr^{5+} are formed when a beam of Kr^{6+} ions with velocity 0.151 a.u. captures a single electron from a Rb $12F$ Rydberg target [5]. Classical trajectory Monte Carlo (CTMC) calculations predict that a narrow range of levels centered around $E\sim -0.25$ eV with a full width at half maximum of about 0.30 eV will be formed in the capture. This is far above the ground level of Kr^{5+} at $E\sim -78.5$ eV [6]. It is expected that the $n=55$ level, with a wide range of L, will constitute approximately 1.7% of the total Rydberg ion population. This relatively selective population mechanism, combined with the efficient detection of $n=55$ levels by CO_2-laser excitation and Stark ionization makes this unusual spectroscopy of high-L Rydberg ion levels possible. One objective of the present study, in addition to the measurement of Kr^{6+} properties, is to explore the factors that determine the signal-to-noise (S/N) ratio in measurements of this type, and other factors constraining the ion species to which this method could be applied.

II. EXPERIMENT

Figure 1 shows a schematic diagram of the apparatus used for this study. A beam of 48.0 keV Kr^{6+} ions ($v=0.151$ a.u.) is obtained from an electron cyclotron resonance ion source. After focusing and charge selection, this beam intersects a Rb Rydberg target, excited to the $12F$ level with three cw lasers [5]. In passing through the Rydberg target, approximately 5% of the Kr^{6+} beam captures a single electron, forming a beam of highly excited Kr^{5+} ions. Immediately following the Rydberg target, both Kr^{5+} and remaining Kr^{6+} ions pass through an einzellens that is adjusted to focus the Kr^{5+} beam. This has the effect of defocusing the remaining Kr^{6+} beam, though it does not completely block it. It also ionizes any Kr^{5+} ions that are formed in extremely high levels ($n>90$). A pair of steering plates following this lens allows correction of the beam steering to compensate for any deflection in the lens. Before entering the laser interaction region, the beam passes through another lens electrode,

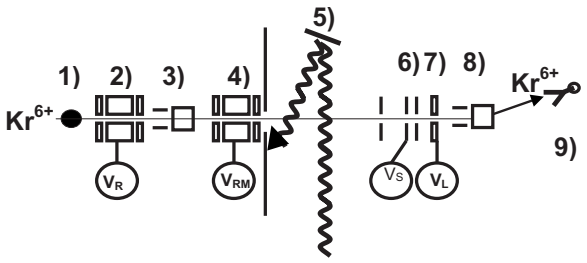

FIG. 1. Schematic diagram of the apparatus used for this measurement. A beam of Kr^{6+} ions intersects a Rb Rydberg target at (1), and a fraction of these ions capture a single electron to become highly excited Rydberg states of Kr^{5+}. A lens at (2) focuses the Kr^{5+} beam and ionizes very weakly bound Kr^{5+} ions. The Rydberg ion beam then passes through a pair of beam steerers and an optional second lens. At (5) a fixed frequency CO_2 laser intersects the ion beam at a variable angle to produce Doppler-tuned excitation from $n=55$ to $n=109$. Any Kr^{5+} ions excited to $n=109$ are Stark ionized at (6), focused at (7), and deflected into a channel electron multiplier at (9). The spectrum of 55-109 excitations is observed by measuring the Stark ionized Kr^{6+} flux as a function of the Doppler-tuning angle.

where an optional field may be applied. The laser interaction region is constructed within a 6 inch Conflat cube. A ZnSe window on the bottom of the cube, antireflection coated at 10.6 μm, admits the CO_2 laser beam. The laser beam crosses the Rydberg ion beam at approximately 90° and then is reflected by a rotatable mirror to intersect the ion beam again at a variable angle. The interior of the cube is enclosed in a mumetal shield, reducing the earth's magnetic field by more than an order of magnitude. The CO_2 laser is a coherent GEMSelect50, which produces a 50 W cw beam at a grating selectable wavelength with a passive frequency stability of 10 MHz. The beam is shaped with a ZnSe lens to produce a 3.7 mm beam radius at the intersection with the Rydberg beam. The laser power is sufficient to saturate the 55-109 transition, exciting close to 50% of the eligible ions. Any Rydberg ions excited in the CO_2 laser will be ionized in the next electrode structure. It consists of two regions of longitudinal electric field. The second region's field is approximately three times that of the first. The negative potential applied to the central electrode (V_S) is chosen so that all Kr^{5+} $n=109$ levels will ionize in the second field but none will ionize in the first. Any Kr^{6+} ions created by this Stark ionization process will be retarded in energy by V_S and can be distinguished from other Kr^{6+} ions that may remain in the beam or that may have been created by other processes somewhere in the beam line. The electric field necessary to ionize all Stark levels of $n=109$ diabatically is approximately [7]

$$E_S \cong \frac{2}{9}\frac{Q^3}{n^4}\ \text{a.u.} \approx 1700\frac{V}{\text{cm}}. \tag{1}$$

This is achieved by applying a potential of −4000 V to an electrode about 2.5 cm away from a grounded electrode. Stark ionized Kr^{6+} ions, decelerated to 44 keV, are deflected upwards into a channel electron multiplier (CEM) at the end of the beamline.

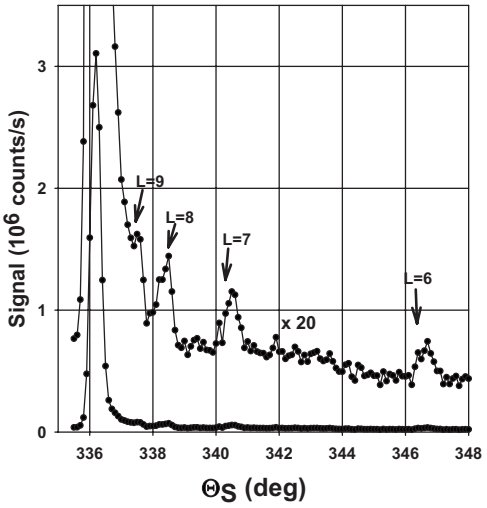

FIG. 2. Typical measured spectrum of 55-109 excitation transitions in Kr^{5+}. The vertical scale is the flux of Stark ionized Kr^{6+} ions produced by the CO_2 laser. The horizontal scale is the reading of the rotation stage controlling the mirror that determines the angle of intersection between the ion and laser beams through Eq. (2). The large peak corresponds to the unresolved excitation of Kr^{5+} ions with $n=55$ and $L>9$ to $n=109$. The 20× magnified signal shows four resolved transitions corresponding to the excitation of $n=55$, $L=6$, 7, 8, and 9 levels to $n=109$.

To observe the 55–109 excitation transition, the CO_2 laser is operated on the $10R(16)$ line at 973.2885 cm^{-1} and the angle of intersection (measured from antiparallel) is scanned over a range of about 15° near 80°. The laser is chopped at a frequency of 2 kHz and the ion signal synchronous with this modulation is detected with a lock-in amplifier. Figure 2 shows an example of the measured signal as a function of the mirror angle. The large peak represents the unresolved excitation of high-L $n=55$ levels to $n=109$. In addition to the full-scale signal, Fig. 2 also shows a 20× magnified signal that reveals partially resolved fine structure at slightly higher frequencies than the high-L peak. These peaks, from right to left, correspond to the excitation and ionization of $n=55$, and $L=6$, 7, 8, and 9 levels. The vertical scale in Fig. 2 measures the count rate produced by the CO_2 laser. The horizontal scale is the reading of the rotation stage controlling the mirror used to vary the angle of intersection between the ion and laser beams. The intersection angle, measured from antiparallel, is given in terms of the rotation stage angle θ_S by

$$\theta = 90° - 2(\theta_S - \theta_\perp), \tag{2}$$

where $\theta_\perp$, the stage angle giving $\theta=90°$, is determined approximately (±0.5°) by observation of the retroreflected laser beam and more precisely using the high-L line position as a calibration. The Doppler-tuned laser frequency is given by

$$\nu_L' = \nu_L \frac{(1+\beta\cos\theta)}{\sqrt{1-\beta^2}}, \tag{3}$$

where ν_L is the fixed laser frequency and $\beta=v/c$, where v is the ion beam velocity.

Because of the small size of the resolved signals shown in Fig. 2, it is of interest to consider the factors contributing to the signal size and to the noise level. The vertical scale in Fig. 2 has been converted from the lock-in signal size to an approximate rate of ion detection with the CO_2 laser on. This conversion relies on an estimate of the gain "g" of the CEM, the net efficiency of converting Kr^{6+} ions entering the CEM into electrons exiting the CEM. Based on manufacturer's data for the CEM (Burle Model 4716) we take this efficiency to be 10^4 at the 1100 V operating voltage of the CEM for incident Kr^{6+} ions at 44 keV. Using this value of g, the background count rate with the CO_2 laser off is estimated to be 3.0×10^6 s^{-1}, slightly smaller than the maximum rate due to the CO_2 laser when it is tuned to the peak of the high-L signal. Since the resolved signals are less than 1% of the high-L signal, they are also less than 1% of the background rate, and noise in the background rate will determine the S/N ratio in the measurement of the resolved signals. The noise spectrum in the signal current from the CEM was examined with an audio spectrum analyzer and found to be relatively flat in the region above 1 kHz. At the 2 kHz modulation frequency of the laser, it would be limited by shot noise in the detected ion flux. If shot noise is the only contributor to the noise, and if B is the background rate and S the signal rate, then the expected S/N ratio in a measurement averaged over a time T is given by

$$\frac{S}{N} \geqslant \frac{\frac{1}{2}ST}{\sqrt{BT+\frac{1}{2}ST}} \tag{4}$$

For one of the resolved peaks in Fig. 1, taking $S=35$ kHz, $B=3.0$ MHz, and $T=45$ s, this predicts S/N ratio ~67. The observed S/N ratio is about a factor of 10 less than this. This indicates that other sources of noise in the background, such as beam and Rydberg target instability are still contributing to the noise. Whether due to fluctuations or shot noise, the S/N would be expected to improve with reductions in the background rate. At present, the dominant source of the background appears to be the ionization of Rydberg ions in the Stark ionizer, since the background rate shows a similar dependence on detector tuning voltages as the 44 keV signal ions. This could indicate that Rydberg levels emptied in the einzellens following the Rydberg target are being repopulated before reaching the detector, possibly by collisional redistribution from lower n levels.

The expected size of the high-L signal is given by

$$S_{HL} = R_p f_{cap} f_{55} T_{ex} \varepsilon_D, \tag{5}$$

where R_p is the flux of the primary beam Kr^{6+}, f_{cap} is the fraction of the primary beam capturing an electron in the Rydberg target, f_{55} is the fraction of the captures that result in a Kr^{5+} in the $n=55$ level, T_{ex} is the excitation probability in the CO_2 laser, and ε_D is the detection probability, the net probability of Stark ionization and collection in the CEM. The primary beam flux should include only that fraction of the beam that falls within the collimation restrictions downstream of the Rydberg target. This is limited by a 6-mm-diam aperture on the first electrode of the Stark ionization detector that occurs about 2 m downstream of the Rydberg target. Even after adjusting the first lens to optimize transmission of the primary beam, only about 5% of the total beam measured at the target is transmitted to the CEM. For the measurements of Fig. 2, we estimate that $R_p=1.1\times10^{10}$ s^{-1}. The capture fraction, f_{cap}, is estimated at 5%, and the fractional population in $n=55$, f_{55}, is estimated from CTMC simulations as 1.7%. The high-L signal rate, estimated assuming $g=10^4$ for the CEM, is 3.2×10^6 s^{-1}. Substituting these estimates into Eq. (5) leads to the estimate

$$T_{ex}\varepsilon_D \cong 0.34. \tag{6}$$

This is close to the maximum possible efficiency. The efficiency of Stark ionization and collection is expected to approach 100%, but the laser excitation efficiency is limited to 50%, even if the excitation transition is fully saturated. Measurements of the high-L signal size as a function of the laser power confirm that the signal is fully saturated, and observation of the focused signal ions on a beam viewer (Colutron BVS-1) confirm a tight focus. Both of these observations support the inferred high total detection efficiency.

One might expect the size of the resolved signals relative to the high-L signal to be related to the L distribution in the capture process. For example, the $L=7$ signal size, relative to the high-L signal size, might be estimated as

$$S_{L=7} \approx f_{L=7} e^{-(T/\tau)} S_{HL}, \tag{7}$$

where $f_{L=7}$ is the predicted fraction of the $n=55$ capture going into the $L=7$ level, τ is the radiative lifetime of the $n=55$, $L=7$ level, and T is the transit time between the Rydberg target and the CO_2 laser. This estimate assumes that most of the $n=55$ capture is into states contributing to the high-L signal whose lifetime is large enough that negligible decay occurs between the target and the laser. However, taking an estimate of $f_{L=7}=0.000\,18$ from a CTMC simulation, using $\tau_{L=7}=0.67$ μs, and $T=1.60$ μs leads to an estimate of the ratio between the $L=7$ and high-L signal of 1.6×10^{-5}, much smaller than the observed 1.6×10^{-3}. The larger signal is due to regeneration of the $L=7$ population by Stark mixing in the electric fields applied in the lens electrodes. The initial population distribution is peaked at the lower values of m_L; CTMC simulations predict that 22% is formed in states with $m_L \leqslant 7$. If this population is spread equally among the 55 different values of L within $n=55$ and then has only the time T_2 between the first lens and the CO_2 laser to radiatively decay, the predicted size of the $L=7$ signal would be

$$S_{L=7} \approx f_{m\leqslant7} \frac{1}{55} e^{-(T_2/\tau)} S_{HL}. \tag{8}$$

With $T_2=0.98$ μs, this predicts the $L=7$ signal at 0.09% of the high-L signal, much closer to the observed 0.16%. Furthermore, if an electric field is applied in the second lens assembly, within 0.21 μs of the CO_2 laser, and this field is large enough to totally mix the $n=55$ manifold, then this predicts a $L=7$ signal size of 0.29% of the high-L signal. It was observed that the resolved signal sizes become substantially larger when a field is applied in the second lens assem-

bly, as compared to when no field is applied there. This confirms that Stark mixing is playing an important role in populating the lower L levels that can be resolved in the 55-109 excitation. It also provides an opportunity to estimate the radiative lifetimes of the levels being excited, by comparing the signal sizes with and without the use of the second lens. More details of this measurement are given below.

The linewidth of the excitation resonances is a primary concern, since it limits the number of individual fine-structure levels that can be resolved. In Fig. 1, the widths of the resolved peaks are about 400 MHz, full width at half maximum, and this is not significantly different from the width of the high-L peak. From day to day, the measured linewidths varied in the range 300–450 MHz. A number of different factors could contribute to these widths, giving both homogeneous and inhomogeneous contributions. Each line is an unresolved doublet due to the spin orbit splitting ($<$33 MHz) in the Rydberg level. There are inhomogeneous contributions to the width due to the velocity and angular spread of the Rydberg ion beam. The Doppler-shifted laser frequency is given by Eq. (3), so the linewidths expected from velocity spread and angular spread are

$$\Delta\nu_\beta = \left(\frac{\Delta\beta}{\beta}\right)(\nu_L \beta \cos\theta),$$

$$\Delta\nu_\theta = (\nu_L \beta \sin\theta)\Delta\theta. \tag{9}$$

For the signals of Fig. 2, where $\nu_L = 973.289\ \mathrm{cm}^{-1}$, $\beta = 0.001\,103$, $\Theta = 81.4°$, $\Delta\beta/\beta \leqslant 0.0002$, and $\Delta\Theta \leqslant 0.0015$ radians, this gives $\Delta\nu_\beta = 1$ MHz, $\Delta\nu_\Theta = 50$ MHz, both much smaller than the observed 400 MHz width. This indicates that the primary source of width is homogeneous, as is also suggested by the high excitation probability discussed above. The possible sources of homogeneous width include natural width ($<$1 MHz), transit width ($1/T \sim 50$ MHz), Stark broadening, and collision broadening.

Stark broadening is probably the dominant source of the observed linewidth. Broadening the 55-109 transition to a full width at half maximum of 400 MHz would require an electric field of about 0.10 V/cm at the site of the laser interaction. The motional electric field due to the residual magnetic field in the region is more than a factor of five smaller than this, but other sources of stray field could include charging of nominally conducting surfaces in the interaction region, contact potential differences between different metals in the interaction region, and the space charge fields due to the Rydberg ion beam itself. The space charge fields could be on the order of 0.03 V/cm if there is no space charge neutralization by thermal electrons, and the importance of space charge was indicated by a clear correlation observed between the primary beam intensity and the measured linewidth. Reducing the beam intensity by a factor of 4 reduced the linewidth by about 30%. Another indication of the importance of Stark broadening was obtained by the study of the $n=55$, $L=6$ excitation resonance, the upper state of which was sufficiently separated from the hydrogenic Stark manifold in $n=109$ so that some partial resolution of Stark-induced forbidden transitions could be seen. These were observed to change in intensity over time periods of 20 min, indicating that the stray fields are probably due to charging of nominally conducting surfaces in the laser interaction region and were changing in time. At times when the stray field appeared to be relatively low, the linewidth of the resolved Stark components of this transition became as small as 200 MHz, indicating that additional sources of line broadening may not be much smaller than the dominant Stark width. Additional study will be required to control Stark broadening and identify additional broadening sources.

TABLE I. Conditions of runs used for spectroscopy of $n=55$ levels. The fixed frequencies of the CO_2 lines are $10R(26)$: 979.7054 cm^{-1}, $10R(16)$: 973.2885 cm^{-1}. Column 1 labels the configuration. Most data was taken in configuration A. Column 2 shows the energy of the Kr^{6+} ion beam. Column 3 indicates the excitation transition studied and column 4 shows the CO_2 line used. Columns 5 and 6 show the calculated transition energy and angular position of the high-L transition.

Configuration	Energy (keV)	Transition	CO_2 line	ΔE_{HL} (cm^{-1})	Θ_{HL} (°)
A	48.0	55–109	$10R(16)$	973.4514	81.304
B	21.0	55–109	$10R(16)$	973.4514	76.765
C	48.0	55–110	$10R(26)$	979.4695	102.642

III. MEASUREMENTS

Table I lists three configurations used for measurements of the frequency differences between the resolved lines and the high-L peak. Most measurements were taken in configuration A, with an ion beam energy of 48.0 keV, exciting the 55-109 transition. However, two other configurations, also shown in Table I, were also used for some of the data. In each case, Table I lists the frequency of the CO_2 line used, and the calculated frequency and angular position of the high-L peak (measured from antiparallel). The frequency differences between the high-L peak and the resolved peaks were calculated from the measured angular differences found in fits of the observed spectra using Eqs. (2) and (3). Table II summarizes the measured frequency differences. The uncertainties reflect the scatter of the repeated results, which is somewhat larger than the statistical errors in the fits.

One important systematic correction is the Stark shift of the transition frequency due to stray electric fields. In the absence of such a field, the transition from the $n=55$, $L=6$ state, for example, would proceed to the $n=109$, $L=7$ state. However, if the stray field is sufficient to mix the $n=109$, $L=7$ state either into the high-L manifold above it or into the $L=6$ state below it, the observed transition energy may be shifted either up or down, depending on the strength of the field, the positions of the levels involved, and the other sources of width. Reasonable agreement with the observed shapes of the partially resolved $L=6$ excitation line shapes were obtained in a Stark model with a zero field linewidth of 120 MHz. The Stark model was then used to generate predicted line center shifts as a function of the net width of the

TABLE II. Summary of measured fine-structure intervals and corrections. Column 1 identifies the transition. Column 2 lists the number of independent measurements of the line's position, and column 3 lists the configurations used for those measurements. Column 4 gives the average frequency offset from the high-L transition after correction for estimated Stark shifts. The listed uncertainties are obtained from the repeatability of the position measurements. For comparison, column 5 gives the average Stark shift applied to obtain the results shown in column 4. Column 6 shows the calculated contribution of relativistic effects to the line position. The sum of relativistic and polarization contributions to the high-L peak position is estimated to be 69(14) MHz. Column 7 gives the portion of the frequency offset due to the difference of polarization energies in the lower and upper states of the transition. All results are in megahertz.

Transition	Number of Observation	Configuration	δE_{obs}	ΔE_S	ΔE_{rel}	ΔE_{pol}
(55,6)–(109,7)	4	A	10 898(59)	+5	169	10 798(61)
(55,7)–(109,8)	3	A	4 730(27)	+23	144	4 655(30)
(55,8)–(109,9)	5	A,B,C	2 409(18)	−1	125	2 353(23)
(55,9)–(109,10)	4	A,B,C	1 365(10)	−1	110	1 324(17)

Stark-broadened composite line shape for the $L=6$, 7, 8, and 9 excitation resonances. The predicted shifts were applied as corrections to the measured frequency differences, and are listed in Table II. The corrections were not larger than the statistical errors in the measurements.

We have, to this point, labeled each line according to our best estimate of its identity. However, the line identification is an important issue that must also be discussed. There is no question that we are observing the 55–109 transition, and there clearly is a systematic pattern in the fine-structure energies, but unfortunately, the pattern alone is not sufficient to determine the values of L for each line. Our best estimate is that the four resolved lines represent the excitation of $n=55$, $L=6,7,8,9$ levels. With this assumption, a scaled plot of the fine-structure energies indicates a polarizability of about 2.6 a.u. for the ground state of Kr^{6+}. If we assume instead that the four lines represent the excitation of $L=7,8,9,10$ levels, a similar scaled plot indicates a polarizability of about 3.6 a.u., and if we assume the four lines represent $L=5$, 6, 7, and 8 levels they would indicate a polarizability of about 1.4 a.u. In each case the scaled plot, described below, is approximately linear. Some additional information is therefore required to unambiguously establish the line identifications. For example, an independent estimate of the core dipole polarizability of even moderate precision can clarify the line identification. In the case of Kr^{6+}, there has been a measurement of the lifetime of the first excited $4s4p\ ^1P$ state. The measured lifetime [$t=0.101(10)$ ns [8]] can be combined with the excitation energy of that state (170 835 cm^{-1}) to estimate the contribution to α_d from that single level. The result is 2.52(25) a.u. If, as expected, this single level is the dominant contributor to α_d, this indicates that the first set of line identifications, $L=6$, 7, 8, and 9, is the correct one, and this is the primary justification for our line identifications.

In the absence of other indications of the approximate value of α_d, it would still be possible to set some limits on the identification of the resolved lines by measuring the lifetime of the $n=55$ state being excited. This measurement can be obtained using the fact that full Stark mixing of any population in the $n=55$ manifold occurs in the lens regions through which the beam passes before reaching the CO_2 laser. It was observed that the ratio between a resolved signal (a) and the high-L peak (HL) becomes significantly larger when a strong field is applied in the second lens region, as compared to when this lens is grounded. This is interpreted as being due to the shorter radiative lifetime of the resolved peaks, compared to the average lifetime of the unresolved high-L levels. If ΔT is the transit time between the first and second lens regions, the relative size of a resolved signal with and without the Stark mixing in the second lens region is expected to be given by

$$\frac{\left(\frac{a}{HL}\right)_{OFF}}{\left(\frac{a}{HL}\right)_{ON}} = e^{-\Delta T[(1/\tau)-(1/\tau_{HL})]}, \tag{10}$$

where τ is the radiative lifetime of the $n=55$ state contributing to the signal and τ_{HL} is the effective lifetime of the states contributing to the high-L signal. Table III shows the measured ratios of the $L=8$ peak to the high-L peak at two different beam velocities, and the inferred lifetime of the state in question. For this calculation, the lifetime of the states contributing to the high-L peak is taken to be 7.1 μs, an

TABLE III. Data used to estimate the radiative lifetime of the $n=55$ level producing the peak at 2409 MHz. ΔT is the transit time between the first and second lens assemblies. a is the fitted amplitude of the peak at 2409 MHz and HL is the fitted amplitude of the high-L peak. The ratio between these is given both with the second lens ON and OFF. Column 5 shows the fraction by which the relative amplitude (a/HL) decreases when the second lens electrode is OFF. Column 6 shows the inferred lifetime of the $n=55$ level being excited, from Eq. (10). This is consistent with the calculated lifetime of the $n=55$, $L=8$ state (0.86 μs), supporting the peak identification.

E (keV)	ΔT (μs)	$(a/HL)_{on}$	$(a/HL)_{off}$	Ratio	τ (μs)
21.0	1.16	0.0075(4)	0.0037(16)	0.49(21)	1.32(71)
48.0	0.77	0.0106(14)	0.0042(11)	0.40(12)	0.75(22)
				Weighted average:	0.80(21)

estimate based on equal populations of all states with $L>10$, using the approximate values of hydrogenic lifetimes [9]. The average result from the two velocities is $\tau=0.80(21)$ μs, in good agreement with the estimated lifetime of the $n=55$, $L=8$ state (0.86 μs). Unfortunately, this result is also consistent with the lifetime of the $L=9$ state (1.07 μs) and the $L=7$ state (0.67 μs), so while this also supports the line identification based on the $4p\ ^1P$ lifetime measurement, it would not by itself be sufficient to make an unambiguous identification.

The differences between resolved peak frequency and the high-L frequency is a result of the fine-structure patterns in both the lower and upper states. In each case, the level positions are expected to be given by

$$E(nL) = E^0(n) + E_{rel}(nL) + E_{pol}(nL), \tag{11}$$

where $E^0(n)$ is the nonrelativistic energy of the n level,

$$E^0(n) = \frac{-Q^2}{2n^2}\frac{1}{\left(1+\frac{m_e}{M_I}\right)}\ \text{a.u} \tag{12}$$

$E_{rel}(nL)$ is a relativistic correction,

$$E_{rel}(nL) = \frac{\alpha^2 Q^4}{2n^4}\left(\frac{3}{4} - \frac{n}{L+\frac{1}{2}}\right), \tag{13}$$

in which α is the fine-structure constant and Q is the charge of the Rydberg ion core, and

$$E_{pol}(nL) = -\frac{\alpha_d}{2}\langle r^{-4}\rangle_{nL} - B_6\langle r^{-6}\rangle_{nL} + \cdots. \tag{14}$$

The frequency of the high-L peak is shifted slightly from the naive hydrogenic frequency by relativistic and polarization shifts. These are calculated assuming that the high-L peak corresponds to the excitation of an equal superposition of all $n=55$ levels with $L>9$. With this assumption, the estimated values of ΔE_{rel} and ΔE_{pol} for the 55-109 high-L transition are 29 and 40 MHz, respectively. To account for uncertainty in the composition of the high-L peak, these are considered to be uncertain by 20%. The high-L peak position is given as

$$\Delta E_{HL} = \Delta E^0 + \Delta E_{rel}^{HL} + \Delta E_{pol}^{HL} = \Delta E^0 + 69(14)\ \text{MHz}. \tag{15}$$

The frequency of a resolved transition from $55L$ to $109(L+1)$ would be given by

$$\Delta E_{55L-109(L+1)} = \Delta E^0 + \Delta E_{rel} + \Delta E_{pol}. \tag{16}$$

The measured frequency difference between a resolved transition and the high-L transition would then be given by

$$\delta E_{obs} = \Delta E_{55L-109(L+1)} - \Delta E_{HL} = \Delta E_{pol} + \Delta E_{rel} - 69(14)\ \text{MHz}, \tag{17}$$

where the last term is the estimated shift of the high-L peak discussed above. The dominant term in the line positions ΔE_{pol} is expected to be given by

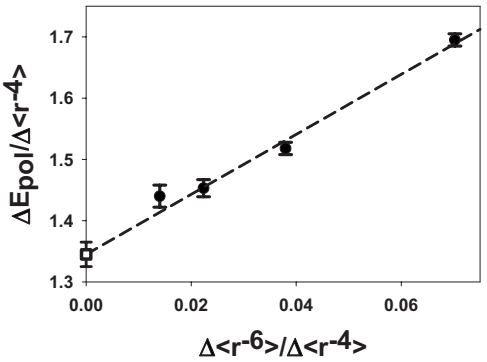

FIG. 3. Scaled plot of the fine-structure energy differences for the four resolved transitions of this study. The vertical axis is the scaled value of ΔE_{pol}, for each transition, from Eq. (20). The dashed line shows a fit to Eq. (16). The fitted intercept, shown by the open square point, determines the dipole polarizability of the Kr^{6+} ion. The fitted slope is related to the quadrupole polarizability, but also contains contributions from other core properties.

$$\Delta E_{pol} = \frac{\alpha_d}{2}\Delta\langle r^{-4}\rangle + B_6\Delta\langle r^{-6}\rangle, \tag{18}$$

where α_d is the core's dipole polarizability and

$$\Delta\langle r^{-4}\rangle = \langle r^{-4}\rangle_{55L} - \langle r^{-4}\rangle_{109(L+1)},$$

$$\Delta\langle r^{-6}\rangle = \langle r^{-6}\rangle_{55L} - \langle r^{-6}\rangle_{109(L+1)}. \tag{19}$$

This suggests plotting

$$\frac{\delta E_{obs} - \Delta E_{rel} + 69\ \text{MHz}}{\Delta\langle r^{-4}\rangle}\ \text{versus}\ \frac{\Delta\langle r^{-6}\rangle}{\Delta\langle r^{-4}\rangle}. \tag{20}$$

to determine both α_d and B_6. Figure 3 illustrates such a plot. The solid points are obtained from the average values of Table II. They were fit to Eq. (18) to obtain best values of the coefficients α_d and B_6. The results of the fit are

$$\alpha_d = 2.69(4)\ \text{a.u.},$$

$$B_6 = 4.90(41)\ \text{a.u.}$$

The fitted value of α_d is a factor of 6 more precise than the estimate based on the lifetime of the $4p\ ^1P$ level. The fitted value of B_6 is related to the quadrupole polarizability of Kr^{6+}, but it also contains contributions from nonadiabatic corrections to the dipole polarizability, and possibly from higher order terms in the interaction between the Rydberg electron and the Kr^{6+} ion. Because of this, additional theoretical input will be required in order to extract a reliable value of α_Q from the fitted value of B_6.

IV. DISCUSSION

The dual goals of this study were to obtain new information about the properties of the Zn-like Kr^{6+} ion and to explore the factors that limit the application of similar techniques to study other multiply charged ions. The new measurement of the dipole polarizabilities of Kr^{6+} satisfy the

first goal with a result nearly an order of magnitude more precise than the value deduced from the $4p\ ^1P$ lifetime [8]. Much higher precision would be possible if microwave techniques, similar to those used in previous RESIS studies of Rydberg ions [2,4] could be used to measure direct transitions between $n=55$ levels of different L. However, such measurements will be difficult without a significant increase in S/N ratio. For example, the $L=7$ peak in Fig. 2 is now seen with a S/N ratio of about 8 in 90 s. A microwave transition would modify this signal by at most 50%.

In principle, the use of Rydberg target capture and CO_2 RESIS excitation could allow the study of fine structures in Rydberg ions of arbitrary charge. In practice, the limiting factor is the S/N ratio. In this study, the noise level is determined by the background level, which is about a factor of 500 larger than a typical resolved excitation signal. This disparity is a symptom of the small size of the resolved signal, about 3×10^{-6} of the primary Kr^{6+} beam current. The small ratio is due to the fact that any particular nL Rydberg level represents a rapidly decreasing fraction of the total Rydberg population as Q increases, typically dropping like Q^{-2}. Still, this would not be such a problem if the background rate could be reduced. Any Rydberg ions formed in ionizable levels should be ionized and removed from the beam in the lens following the Rydberg target. Then, since the detector selects only Kr^{6+} ions ionized in the detector and decelerated by 4 keV, nothing should be detected unless the CO_2 laser excites ions into ionizable levels. In practice, this works only up to a point. From CTMC simulations, it is estimated that 13% of the Rydberg ions formed in the Rydberg target, or about 7×10^7 ions/s, are initially in ionizable levels, yet the background rate is 20× smaller than this. So it seems that the preionization is quite effective, reducing the potential background rate by a factor of 20. This is as expected since the maximum electric field in the lens (2400 V/cm) is substantially larger than the ionizing field in the detector (1600 V/cm). However, it is also clear that the dominant source of background is still ionizable Rydberg levels. A possible source of these ions is collisional repopulation of levels emptied in the lens. Increasing the size of the preionizing electric field to ionize more deeply bound levels and reducing the system pressure (currently about 10^{-8} Torr) may further reduce the background level and increase the S/N ratio. Another approach is to increase the stability of the background rate, since fluctuations in this rate appear to still be a factor in the noise level. With attention to both approaches, significant increases in S/N ratio may be possible.

Another important factor in possible future applications of this technique to study other multiply charged ions is the excitation linewidth. There are likely to be several significant sources of linewidth in such experiments. This study identifies Stark broadening as the dominant source of linewidth, but other sources are not much smaller. Since the principal quantum number of the upper state of a typical RESIS transition scales linearly with Q, Stark broadening, even at a constant value of stray field, will likely increase linearly with Q also. Until efforts to control stray electric fields are exhausted and other broadening mechanisms are fully understood, it will be difficult to predict the resolution limit of other possible studies. Larger linewidths will make it difficult to resolve fine-structure patterns in Rydberg ions in which the core ion does not have relatively large polarizabilities or permanent moments. For example, in Rydberg states built on S-state ions,

$$\langle r^{-4}\rangle \cong \frac{Q^4}{n^3L^5} \quad \text{for } L \ll n, \tag{21}$$

so for a fixed value of L and a constant value of α_d, the size of the scalar fine-structure pattern in the $n=9Q$ level would actually increase somewhat with Q, mitigating the probable linewidth increase. However, in some systems, e.g., helium-like Rydberg ions, where α_d decreases rapidly with Q, the scale of fine-structure patterns will decrease with Q. When combined with the increased linewidth, this will make such studies very difficult. In other cases, such as multielectron multiply charged ions, both the core polarizability and the core charge can be large, making these ions quite susceptible to RESIS studies, even for large values of Q. Since *a priori* calculations of ion properties become more challenging for large nuclear charge and large numbers of electrons, obtaining experimental measurements of the properties of many-electron multiply charged ions appears to be a promising application for the RESIS technique.

ACKNOWLEDGMENTS

This work was supported by the Chemical Sciences, Geosciences, and Biosciences Division of the Office of Basic Energy Sciences, Office of Science, U.S. Department of Energy. The experiments were performed at the J.R. Macdonald Laboratory of Kansas State University.

[1] S. R. Lundeen, in Advances in Atomic Molecular and Optical Physics Vol 52, edited by Paul R. Berman and Chun C. Lin (Academic Press, New York, 2005), pp. 161–208.

[2] R. A. Komara, M. A. Gearba, and S. R. Lundeen, Phys. Rev. A **67**, 062502 (2003).

[3] R. F. Ward, Jr., W. G. Sturrus, and S. R. Lundeen, Phys. Rev. A **53**, 113 (1996).

[4] R. A. Komara, M. A. Gearba, C. W. Fehrenbach, and S. R. Lundeen, J. Phys. B **38**, 587 (2005).

[5] F. J. Deck, E. A. Hessels, and S. R. Lundeen, Phys. Rev. A **48**, 4400 (1993).

[6] NIST atomic spectroscopy database http://physics.nist.gov/PhysRefData/ASD

[7] T. F. Gallagher, *Rydberg Atoms*, (Cambridge University Press, Cambridge, England, 2005).

[8] E. H. Pinnington, W. Ansbacher, and J. A. Kernahan, J. Opt. Soc. Am. B **1**, 30 (1984).

[9] E. S. Chang, Phys. Rev. A **31**, 495 (1985) gives the approximate formula $A(Q,n,L)=(1.08\times10^{10}\ \mathrm{s}^{-1})\frac{Q^4}{n^3(L+\frac{1}{2})^2}$.